Materials Science & Engineering C 118 (2021) 111353

Contents lists available at ScienceDirect

Materials Science & Engineering C

journal homepage: www.elsevier.com/locate/msec

Graphene-laden hydrogels: A strategy for thermally triggered drug delivery

Emanuele Mauri[a], Aurora Salvati[a], Antonino Cataldo[b,c], Pamela Mozetic[d], Francesco Basoli[a], Franca Abbruzzese[a], Marcella Trombetta[a], Stefano Bellucci[b,*], Alberto Rainer[a,d,**]

[a] Department of Engineering, Università Campus Bio-Medico di Roma, via Álvaro del Portillo 21, 00128 Rome, Italy
[b] National Institute for Nuclear Physics (INFN), via E. Fermi 40, 00044 Frascati, Rome, Italy
[c] Department of Information Engineering, Università Politecnica delle Marche, Via Brecce Bianche, 1, 60131 Ancona, Italy
[d] Institute of Nanotechnology (NANOTEC), National Research Council, c/o Campus EcoTekne, via Monteroni, 73100 Lecce, Italy

ARTICLE INFO

Keywords:
Graphene
Hydrogel
Thermally-controlled drug delivery
Diclofenac
Cyclooxygenase

ABSTRACT

The synthesis of graphene-based materials has attracted considerable attention in drug delivery strategies. Indeed, the conductivity and mechanical stability of graphene have been investigated for controlled and tunable drug release *via* electric or mechanical stimuli. However, the design of a thermo-sensitive scaffold using pristine graphene (without distortions related to the oxidation processes) has not been deeply investigated yet, although it may represent a promising approach for several therapeutic treatments. Here, few-layer graphene was used as a nanofiller in a hydrogel system with a thermally tunable drug release profile. In particular, varying the temperature (25 °C, 37 °C and 44 °C), responsive drug releases were noticed and hypothesized depending on the formation and perturbation of π-π interactions involving graphene, the polymeric matrix and the model drug (diclofenac). As a result, these hybrid hydrogels show a potential application as thermally triggered drug release systems in several healthcare scenarios.

1. Introduction

Smart drug delivery systems (DDS) represent a milestone in the development of efficient therapeutic strategies in modern healthcare. Indeed, research has focused on the tunable pharmacokinetics and the efficacy of released active principles, generating a wide range of polymer-based biomaterials. Among them, hydrogels are commonly recognized as tailored three-dimensional (3D) networks to perform sustained drug release. Their unique physical-chemical properties are essentially correlated to the porous structure and the high-water imbibing capacity: they guarantee the diffusion of drug payload and the exchange of ions and metabolites with tissues to maintain the biological chemical balance with the surrounding environment [1]. However, the drug release from these 3D scaffolds is mostly driven by a pure diffusion mechanism, due to the high clearance observed *in vivo* and it cannot be modulated through external stimuli. To overcome these limitations, hybrid composites are being developed and the scientific community has shown great interest in the use of graphene as a nanoscale filler [2,3]. Graphene is defined as a single layer of sp^2-hybridized carbon atoms arranged in a honeycomb two-dimensional (2D) lattice array [4,5]. The application of graphene in the synthesis of drug carriers is justified by its peculiar feature, which include high Young's modulus, mechanical stability, excellent electrical and thermal conductivity, and combination of fast mobility of charge with a large specific surface area that provide multiple attachment sites for drug targeting [6,7]. Indeed, the planar configuration represents an attractive substrate to immobilize different substances, such as drugs, biomolecules, chromophores and cells [8–10]. The main application of graphene in DDS is in its oxidized (graphene oxide, GO) or reduced (reduced graphene oxide, rGO) state to endow polymeric networks with improved mechanical consistence, self-healing ability, ultrasound or IR responsivity, which affect the drug release kinetics [11,12]. In particular, the choice of graphene oxide is due to its water dispersibility, result of the epoxide and hydroxyl functionalities on the two sides of a single layer of graphene, and of the carboxylic terminal groups at the edges: the polarity of these chemical groups empowers the formation of hydrogen bonds with hydrophilic molecules and their chemical reactivity gives rise to covalent linkage with polymers or biomolecules [13,14]. For example, Dembereldorj and coworkers [15] have proposed the PEGylation of GO to optimize the biocompatible release of doxorubicin; Wang et al. [16] discussed the covalent functionalization among GO and polyethyleneimine, polyethylene glycol, and folic acid to design a plasmid

* Correspondence to: S.Bellucci, National Institute for Nuclear Physics (INFN), via E. Fermi 40, 00044 Frascati, Rome, Italy
** Correspondence to: A. Rainer, Department of Engineering, Università Campus Bio-Medico di Roma, via Álvaro del Portillo 21, 00128 Rome, Italy.
E-mail addresses: bellucci@lnf.infn.it (S. Bellucci), a.rainer@unicampus.it (A. Rainer).

https://doi.org/10.1016/j.msec.2020.111353
Received 9 April 2020; Received in revised form 8 July 2020; Accepted 30 July 2020
Available online 11 August 2020
0928-4931/

delivery system for targeting hepatocellular carcinoma; Cheng and coworkers [17] described the synthesis of a 3D printable GO-hydrogel as a BMP7 protein delivery system to protect cartilage by influencing the Rank/Rankl/OPG pathway *in vitro* and *in vivo*. On the other hand, the application of pristine graphene is investigated due to its specific conductivity (higher than its oxidized derivative) and mechanical stability: recently, González-Domínguez et al. [18] have studied the response of a hybrid graphene-hydrogel to electrical and mechanical stimuli to modulate the release of a drug. However, the thermal behavior of pristine graphene within a polymeric matrix has not been fully investigated yet. The thermal triggering approach to drug delivery is common in cancer [19–21] and brain tumors [22,23]. In this work, we propose the synthesis of graphene-based hydrogels as thermo-sensitive carriers for controlled drug release. Hydrogels were obtained *via* microwave-assisted condensation reaction between branched polyacrylic acid and agarose, and pristine nano-layered graphene (few-layered graphene, FLG) was used as a nanofiller to investigate the graphene thermal effect in the drug release scenario. The use of microwave irradiation is justified by its main benefits compared to other common routes used in the synthesis of three-dimensional polymeric scaffolds [24,25]. It ensures short reaction time, absence of organic solvents and potential toxic cross-linkers, limited side reactions and minimal amounts of unreacted species [26,27]. The FLG stabilization was obtained through the dispersion of exfoliated graphite in isopropyl alcohol to induce the intercalation of the solvent molecules into the graphitic interlayer spaces, providing a material with increased water dispersibility. This approach ensures the *sol-gel* transition in aqueous media, avoiding the use of organic solvents. Moreover, the synthetized hybrid scaffolds preserve all the peculiar features of pristine graphene, without distortions related to the oxidation processes. We investigated the drug release profile at three different temperatures: 25 °C (room temperature), 37 °C (physiological condition) and 44 °C (a value associated with hyperthermia treatments [21]). Diclofenac, an anti-inflammatory molecule commonly used to treat musculoskeletal and systemic inflammations, was chosen as a candidate drug preserving its bioactivity in the investigated temperature range [28,29]. Results showed tunable diclofenac release over time, according to the temperature increase. This response was not observed in polymeric scaffolds without FLG, suggesting that the thermal response and the π-conjugated structure of the nanofiller [30,31] affected the electrostatic interactions with drug and, hence, its release kinetics. In particular, by increasing the temperature, the release of diclofenac became faster. Furthermore, we evaluated the anti-inflammatory performance of the released drug in terms of cyclooxygenase (COX) inhibition, reporting an efficiency comparable to that of its analytical standard, thereby proving that the interaction with FLG did not alter the drug. According to ISO 10993-5, these graphene hybrid hydrogels present high biocompatibility, supporting their potential application for thermally triggered drug release in several biomedical applications.

2. Experimental

2.1. Materials

Branched polyacrylic acid (carbomer 974P, MW = 1 MDa, Fagron) and ultrapure agarose (MW = 200 kDa, Thermo Fisher Scientific) were used as reagents for gel formulation. Commercially available intercalated graphite was provided by Asbury Carbons (Anthracite Industries, Inc.) and was used as the starting material for the synthesis of FLG. This graphite was intercalated with sulphates and nitrates, positioned between the various carbonaceous layers, and prepared in acidic environment (pH between 1 and 6). All other chemicals and diclofenac sodium salt were purchased from Merck KGaA. The materials were used as received, without further purifications, and the solvents were of analytical grade.

2.2. Synthesis of few layered graphene (FLG)

FLG were fabricated through the exfoliation method assisted by microwave irradiation, according to a simple and industrially scalable procedure [32,33] previously developed at the INFN NEXT Nanotechnology Laboratory in Frascati (Rome). Intercalated graphite (2 g) underwent a sudden thermal shock for 30 s, caused by microwave irradiation (800 W), and resulting in a growth temperature above 1000 °C. The resulting crystalline stacks of atomic graphene layers (200 mg, hereinafter FLG) were dispersed in isopropyl alcohol (200 mL) by stepwise additions (50 mg each) every 10 min under pulsed-mode sonication at room temperature (RT), to a final concentration of 1 mg/mL. The obtained system was dried at 90 °C to remove alcohol and the resulting agglomerate was dispersed in distilled water at 0.01% w/v and sonicated for 40 min, until complete suspension. Scanning electron microscopy (SEM) analysis of FLG specimen was performed on a Tescan Vega II microscope, endowed with a tungsten filament.

2.3. Synthesis of graphene-laden hydrogels

The starting branched polyacrylic acid (PAA) solution was prepared as follows: carbomer 974P (50 mg) was dissolved in PBS solution (9.95 mL), then the mixture was left to settle for 30 min and pH was brought to 7.8 by 1 M NaOH addition. Hence, graphene-laden hydrogels (FLG-HG) were synthetized: agarose (40 mg, 0.8% w/v) was added to PAA solution (5 mL) and the mixture was exposed to microwave stimulation (500 W) for 30 s and heated to 80 °C to induce the condensation reaction between the carboxyl and hydroxyl groups. The reactor was kept closed to prevent solvent evaporation. The resulting system was cooled to 60 °C and mixed at 1:1 volume ratio with the FLG solution, obtaining a final FLG concentration of 0.5 mg/mL. Finally, the solution was vortexed (20 s) obtaining a homogenous mixture and cast in cylindrical molds (diam 1.1 cm, 250 μL per mold) upon cooling to achieve the complete gelation (in about 6 min, as monitored using the inverted tube test, Supplementary material). Pristine hydrogels (HG) were also produced as a reference standard for the experimental validations. The latter were synthetized following the FLG-HG protocol using distilled water for the 1:1 dilution stage prior to casting.

2.4. Water uptake behavior

Water uptake capacities of FLG-HG and HG were evaluated gravimetrically. The hydrogel samples were first immersed in PBS for about 30 min, to remove potential unreacted components, and freeze-dried; then they were weighed (W_{dry}) incubated in excess PBS (about 3 mL) to reach complete swelling. At defined time points, each sample was removed from the PBS, wiped with moistened filter paper and weighed (W_{wet}). The water uptake percentage (Q) was calculated according to Eq. (1):

$$Q = \frac{W_{wet} - W_{dry}}{W_{dry}} \times 100\% \quad (1)$$

Data were recorded at temperatures of 25 °C, 37 °C and 44 °C and each condition was analyzed in triplicate.

2.5. Characterization techniques

2.5.1. Raman spectroscopy

Raman characterization was carried out using an Invia microscope (Renishaw) equipped with a 532 nm laser and two gratings (600 and 1800 lines/mm). Spectra were acquired directly on the lyophilized samples. The power laser, the exposure time and the number of accumulations were optimized for each sample.

2.5.2. FT-IR analysis

FT-IR analysis was performed on an Agilent Cary 630 spectrometer, equipped with Diamond ATR-module, at a resolution of 2 cm^{-1} and 128 acquisitions. Lyophilized samples were placed on the diamond cell without any preparation, and spectra were recorded in the 4000–650 cm^{-1} wavenumber range.

2.5.3. Rheological characterization

Measurements were performed on a MCR302 rheometer (Anton Paar GmbH) with a 25-mm plane plate configuration. Amplitude sweep and frequency sweep tests were conducted at 25 °C, 37 °C and 44 °C, after complete gelation of each sample. Amplitude tests were performed at 10 Hz, whereas G′ (elastic modulus) and G″ (loss/viscous modulus) were determined at low strain values (0.1%) over the frequency range 0.5–50 Hz.

2.6. Drug loading

Drug loading was performed during the synthetic step. Diclofenac was respectively dissolved in FLG solution (FLG-HG group) or in distilled water (HG group) at 0.5 mg/mL. The drug solution was sonicated for 1 h at room temperature (RT) and added to the polymeric mixture post-microwave irradiation at a 1:1 volume ratio, leading to a final drug concentration of 0.25 mg/mL in the hydrogel samples. The addition of FLG-drug (or drug alone) occurred during the cooling of the polymeric system, at 60 °C. Complete gelation was achieved in cylinders in *ca.* 6 min, as described above.

2.7. Drug release profiles

Drug release mechanism was investigated at pH 7.4, at different temperatures: 25 °C, 37 °C and 44 °C. In details, hydrogel specimens were incubated in PBS (1 mL) and 500 μL aliquots were collected at defined time points up to 96 h, restoring the buffer volume to avoid mass transfer equilibrium with the surrounding environment. The amount of released diclofenac was determined by UV–vis spectroscopy at $\lambda = 276$ nm against a calibration curve.

2.8. Cytotoxicity assay

The biocompatibility of HG and FLG-HG was assessed *in vitro*, according to ISO 10993-5, using BALB/3T3 cell line (American Tissue Culture Collection, ATCC). Lyophilized hydrogel specimens were sterilized by UV irradiation for 20 min and placed into a 24-well plate. Then, Dulbecco's Modified Eagle Medium (DMEM) supplemented with 10% fetal bovine serum (FBS), 1% L-glutamine, and 1% penicillin/streptomycin (Merck KGaA) were added to each sample (1 mL per 3.5 mg of hydrogel specimen) and incubated for 24 h at 37 °C. The resulting eluate was supplemented to cell cultures at different titers and cell viability was evaluated at 24 h by MTT assay, which is based on the reduction of tetrazolium salts by metabolically active cells. Briefly, 3-(4,5-dimethylthiazolyl-2)-2,5-diphenyltetrazolium bromide was added to each well to a final concentration of 0.5 mg/mL. After incubation for 4 h at 37 °C, 5% CO_2, medium was removed, and the resulting intracellular purple formazan salts were dissolved in DMSO (200 μL per well). Absorbance was measured at 590 nm on a microplate reader (TECAN M200 Pro plate reader). Non-treated cells were used as a control for cell viability. Experiments were performed in triplicate.

2.9. Cyclooxygenase (COX) assay

The anti-inflammatory activity of diclofenac following its release from the hydrogels was tested *in vitro* in terms of COX inhibition on cell lysates. The THP-1 monocytic cell line was used as a cell model. Cells were maintained in RPMI 1640 (Merck KGaA) supplemented with 10% fetal bovine serum (FBS), 1% non-essential amino acids, 1% sodium pyruvate and 0.1 mg/ml penicillin/streptomycin/L-glutamine (Merck KGaA). Cell differentiation into macrophages was performed in 75 cm^2 flasks at a density of 1×10^6 cells/mL in complete RPMI containing 150 nM phorbol 12-myristate 13-acetate (PMA) (Merck KGaA). Medium was changed after 24 h, and cells were cultured for additional 48 h in complete RPMI. Inflammation was induced by administration of 10 ng/mL LPS (Merck KGaA) for 48 h. Cells were then washed with PBS and detached by trypsin. THP-1 macrophages were pelleted by centrifugation at 200 $\times g$ for 5 min and washed with PBS. The pellet was lysed in a lysis buffer consisting of ice-cold PBS, 1% NP-40 surfactant (Thermo Fisher Scientific) and Halt Protease Inhibitor Cocktail (1:1000, Thermo Fisher Scientific), and incubated on ice for 5 min. The lysate was centrifuged at 13,000 $\times g$ for 5 min at 4 °C and the supernatant was collected.

Inhibitory effect of diclofenac was analyzed through a Fluorometric COX Activity Assay (Abcam, ab204699), representing a sensitive method to detect the peroxidase activity of COX in biological samples. Eluates from FLG-HG were withdrawn after 24 h incubation, and diclofenac concentration was determined spectrophotometrically. A freshly prepared diclofenac solution, at the same concentration, was used as a positive control. Additionally, a no-drug group was used for data normalization.

In our typical experiment, 20 μL of reaction buffer containing cell lysate, fluorometric probes and sample under investigation were spotted on a 96 well multiplate. After the addition of arachidonic acid (COX substrate) in NaOH solution, the enzymatic reaction led to the production of a fluorescent molecule (resorufin dye, $\lambda_{Ex/Em}$ = 535/587 nm), that could be monitored in kinetic mode (one read every 15 s) for 20 min at RT, using a TECAN M200 Pro plate reader. Data were plotted as Relative Fluorescence Units (RFU) over time and COX activity could be determined as the slope of the curve in its linear region, using a resorufin standard calibration curve: in particular, 1 COX unit is defined as the amount that leads to the production of 1 μmol of resorufin per min, at physiological pH and 25 °C.

2.10. Statistical analysis

Where applicable, experimental data were analyzed using Analysis of Variance (one-way and two-way ANOVA). Statistical significance was at the 0.05 level. Results are presented as mean value ± standard deviation.

3. Results and discussion

3.1. FLG production

FLG was prepared using an expandable graphite characterized by intercalating sulfate and nitrate derivatives, localized among the graphite planes. The microwave-induced thermal shock promotes the intercalating substances vaporization, which modifies the air dielectric properties and causes a propagation of sparks that sustain the process, reaching temperatures around 1000 °C [34]. During the vaporization, the gases exert a pressure between two adjacent planes increasing the reciprocal distance and giving rise to the final exfoliated material. The resulting graphene presented a worm-like structure, with a higher surface area and a thickness in the range of 3–9 planes, according to the expansion process. Therefore, the material has the ability to increase the electronic interactions with other molecules, exploiting its cyclic nature and the electronic cloud that can merge with other rings or protonated/deprotonated chemical groups [35,36]. Moreover, the use of microwave irradiation ensures a fast and cheaper procedure in terms of time (30 s) and energy needs (lower than a thermal approach carried out in an oven), and the experimental conditions are solvent-free, reducing potential side effects and secondary reactions. The subsequent formation of nanoplatelets occurred as dispersion in isopropyl alcohol, under ultrasound, that ensures the rearrangement of graphene layers to

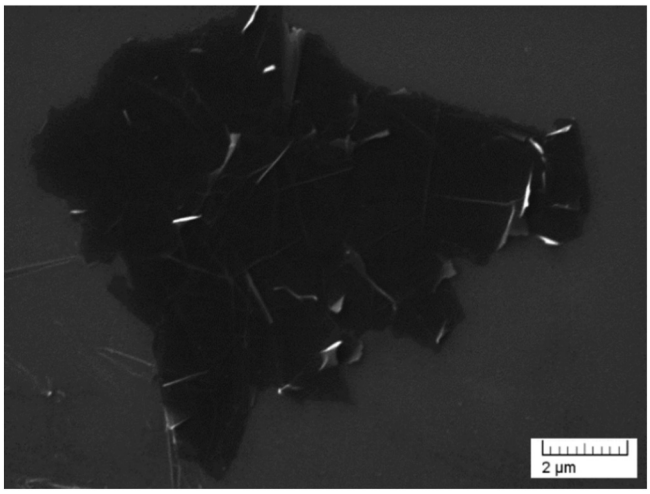

Fig. 1. Scanning electron micrograph of graphene nanoplates.

form nanostructures with the two-dimensional lateral sides having sizes of about 10 µm, as shown in Fig. 1, and a thickness of 5 nm.

Isopropyl alcohol is less aggressive than other commonly used solvents, protects graphene against chemical modifications or aggregations and ensures the FLG stabilization in aqueous medium due to the interactions between its hydroxyl groups and the graphene π-surface or the edges, preserving the thermal properties of the material [37–39]. The resulting FLG was characterized by high graphitic sp^2 character and the presence of oxygenated groups was negligible [33,40,41].

3.2. Hydrogel formation

The gelation mechanism of our material is due to the chemical cross-linking between the carboxyl groups of polyacrylic acid and the hydroxyl moieties of agarose. The microwave irradiation causes a temperature increase to *ca.* 80 °C, enhancing the macromer mobility, and thus the short-range interconnections among functional groups of the polymers. This leads to the production of local networks (also known as microgels) which, as polycondensation proceeds, give rise to the final hydrogel matrix. During the *sol-gel* transition, the viscosity progressively increases, decreasing the mobility of macromers and allows closer functional groups still react efficiently. The resulting physico-chemical condition promotes the 'welding' between microgel surfaces, giving rise to the three-dimensional macrostructure [42]. The choice to use carbomer and agarose was due to their well-known biocompatible features that make them good candidates in therapeutic protocols and tissue engineering: carbomer also possesses an anti-inflammatory action [43,44], and agarose shows tunable properties suitable for medicine-oriented applications, such as permeation to oxygen and nutrients, resemblance to extracellular matrix components and low immunogenicity [45,46]. Furthermore, the microwave-assisted approach ensures the design of hydrogels able of *in situ* forming, offering a major advantage over rigid scaffolds because they can easily adapt to any shape and can also be introduced using minimally invasive procedures. In this work, the hydrogel building blocks were made up mostly of C—C bonds, where FLG was entrapped through physical interactions, without affecting the peculiar properties of graphene, as shown in Fig. 2. For these reasons, FLG was added after microwave irradiation, during the *sol-gel* transition. Similarly, the drug was firstly added to the FLG solution and added to the polymer solution following microwave irradiation, in order not to affect the reciprocal interactions between diclofenac and FLG. In particular, the drug molecules non-covalently adsorb onto or wrap around the graphene surface, due to the π-π and physical bonds formation (Supplementary material). Indeed, the covalent functionalization of graphene generally include two different routes: the formation of covalent bonds between free radicals or dienophiles and C=C bonds of the pristine graphene or between organic functional groups and the oxygen groups of graphene oxide [2,47].

SEM analysis (performed on fracture surfaces of lyophilized samples, and included as Supplementary material) confirmed homogeneous FLG dispersion in the HG matrix, ruling out the presence of FLG agglomerates.

Raman analysis, in Fig. 3, shows the spectra of neat and graphene-laden hydrogels. In pristine HG (Fig. 3A), the signal at 3438 cm^{-1} can be ascribed to the stretching vibration of the residual O—H groups, whereas the peak at 2954 cm^{-1} is related to the C—H stretch of the polymer backbone. The formation of ester bonds can be traced back to the asymmetric CO_2 stretching at 1476 cm^{-1} and to the C—O—C stretch vibration in the range 900–1000 cm^{-1}, which can be ascribed to the glycosidic bond between the monosaccharide units of agarose and the formed ester groups.

The Raman spectrum of FLG-HG (Fig. 3A) shows all the peculiar peaks of pristine HG (the O—H stretching at 3471 cm^{-1}, the C—H stretching at 3000 and 2950 cm^{-1}, and the asymmetric CO_2 stretching of esterification at 1465 cm^{-1}), even if partially covered by graphene bands (D band = 1353 cm^{-1}, G band = 1585 cm^{-1} and 2D band = 2718 cm^{-1}), suggesting that the FLG intercalation did not chemically modify the hydrogel matrix and the graphene layers were entrapped within the mesh size through physical bonds. An additional check was carried out through ATR/FT-IR analysis, that ensured a clear detection of the characteristic peaks of chemical cross-linking between carbomer and agarose, and the absence of chemical shift following the embedding of FLG (Supplementary material).

Nevertheless, a furthered analysis of O—H and C—H bond stretching confirms the nature of interaction between FLG and hydrogel matrix. The intermolecular interactions occurring in the studied system can be divided into two main groups: site-specific polar (polar π interaction, in our case hydrogen bonding due to hydroxyl and carboxylic groups) and non-specific dispersive interactions (London–van der Waals interactions, related to C—H instantaneous dipole moments). The two types of interactions are highlighted by the change in relative intensity of O—H and C—H bond stretching. In Fig. 4A, the normalized intensity and peak area of C—H stretching at 3000 cm^{-1} and O—H stretching at 3471 cm^{-1} are reported *vs.* peak at 2950 cm^{-1}, which was set as internal reference. This evaluation demonstrated that FLG was physically entrapped in the hydrogel matrix generating intramolecular interaction with the polymer. The presence of FLG promoted the dispersive interaction, as detectable by the increased value of the 3000 cm^{-1}/2950 cm^{-1} ratio, both in intensity and peak area, in FLG-HG (Fig. 4A, black columns) compared to the neat hydrogel matrix (Fig. 4A, red columns), and hinder the polar interactions resulting in the decreasing of the value of the 3471 cm^{-1}/2950 cm^{-1} ratio, both in intensity and peak area, in FLG-HG (Fig. 4A, black columns) compared to HG (Fig. 4A, red columns). This is in agreement with previous literature (Belyaeva and coworkers [48]) that shows how the transparency of FLG to polar and dispersive interactions may vary upon the nature of the supporting substrate, as well as the number of graphene layers and the presence of contaminants and defects at the FLG/substrate interface. In particular, in the presence of corrugations in the FLG structure (as reliably occurring in our system), FLG is reported to screen polar interactions, while transmitting dispersive ones.

The reciprocal π-π and physical interactions between diclofenac and graphene are confirmed by a shift of the G band, as reported in Fig. 4B. The G-band of pristine FLG, located at 1581.45 ± 0.06 cm^{-1}, experiences a shift of 1.3 cm^{-1} due to the interaction with diclofenac, proving the carrier-drug bond through π-π interactions.

3.3. Hydrogel physical properties

The peculiar feature of hydrogels is their capacity to retain a high amount of water and ensure exchange and diffusion of molecules with

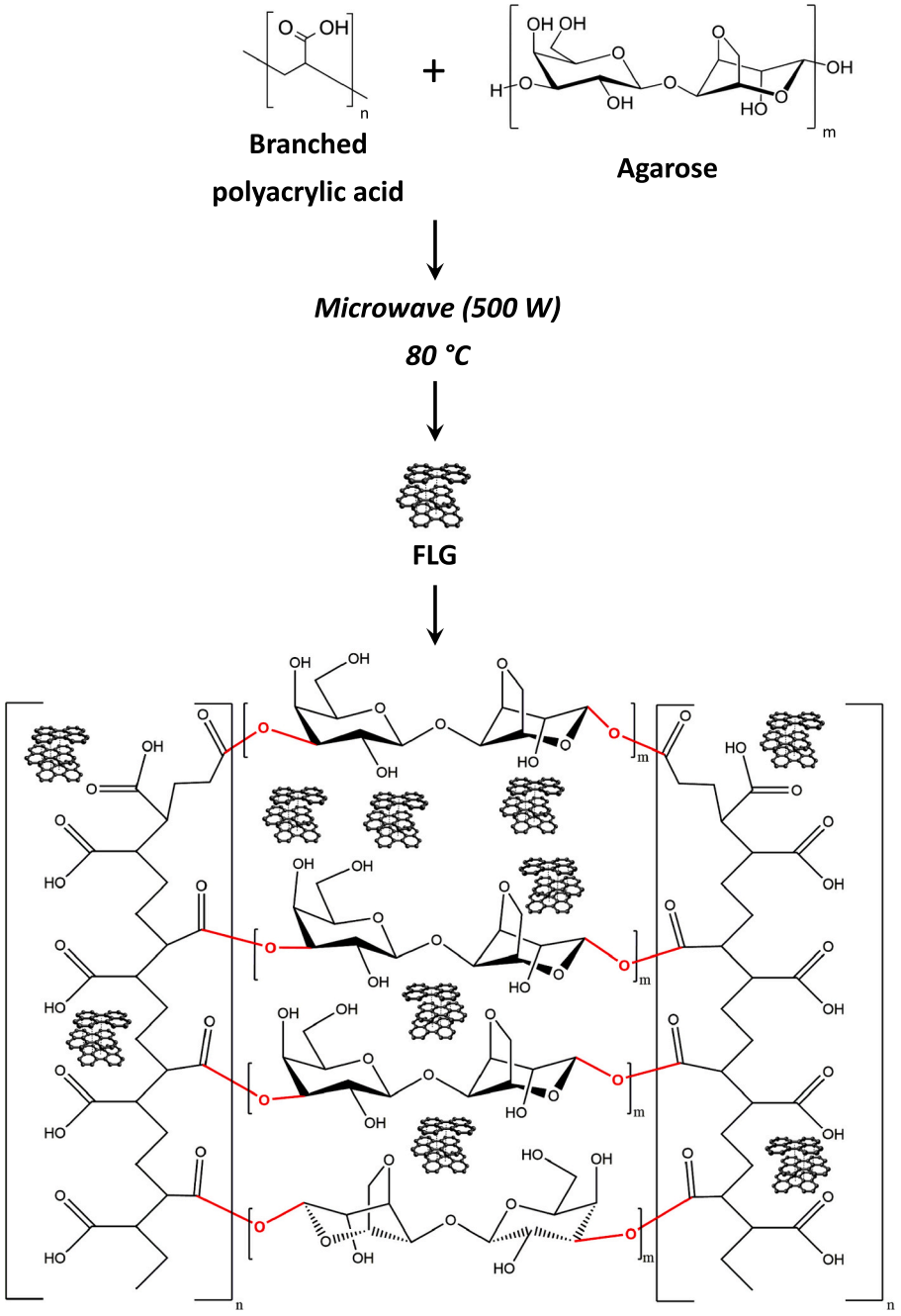

Fig. 2. Synthesis of graphene-laden hydrogel and putative matrix chemical structure: ester bonds (cross-linking points) are highlighted in red. (For interpretation of the references to color in this figure legend, the reader is referred to the web version of this article.)

the surrounding environment. The water uptake capacity is a function of the network structure, in terms of concentration of the elastic chains, hydrophilicity, density of electronic charge of the functional groups, and pore size [49]. The addition of FLG could affect the polymer chains stretching during the exposure to aqueous solvents, altering the swelling and the equilibrium water content. We investigated this aspect at different temperatures and compared the FLG-HG samples to those pristine HG. As shown in Fig. 5, HG shows higher water uptake at equilibrium than FLG-HG at 25 °C (6300 ± 200% *vs.* 5000 ± 200% after 24 h). At 37 °C and 44 °C, instead, HG and FLG-HG show similar trends and reach the same swelling equilibrium, with FLG-HG only showing an increased water uptake *vs.* pristine HG in the initial phase of swelling. These results could be explained considering the nature of FLG: at RT, its hydrophobicity and the physical interaction between the π-system and the residual hydroxyl and carboxyl groups counterbalances the polymer chains elongation, resulting in an opposite force to the swelling; increasing the temperature, the mobility of cross-linked polymer tends to increase and the thermal transfer ability of FLG [50] supports the scaffold stretching, also inducing a more swollen configuration in the first minutes at 44 °C. Therefore, the presence of FLG results in a temperature-dependent modulation of the initial hydrogel swelling behavior. Generally, the equilibrium between the hydrophobic and hydrophilic polymer moieties controls the water uptake ability of the hydrogel [51,52]: here, the presence of graphene nanofiller contributes to the definition of the equilibrium state in aqueous medium.

Rheological studies were carried out to characterize the viscoelastic behavior of the hydrogel samples. Notably, the FLG loading could affect the scaffold capacity to store energy elastically, promoting a

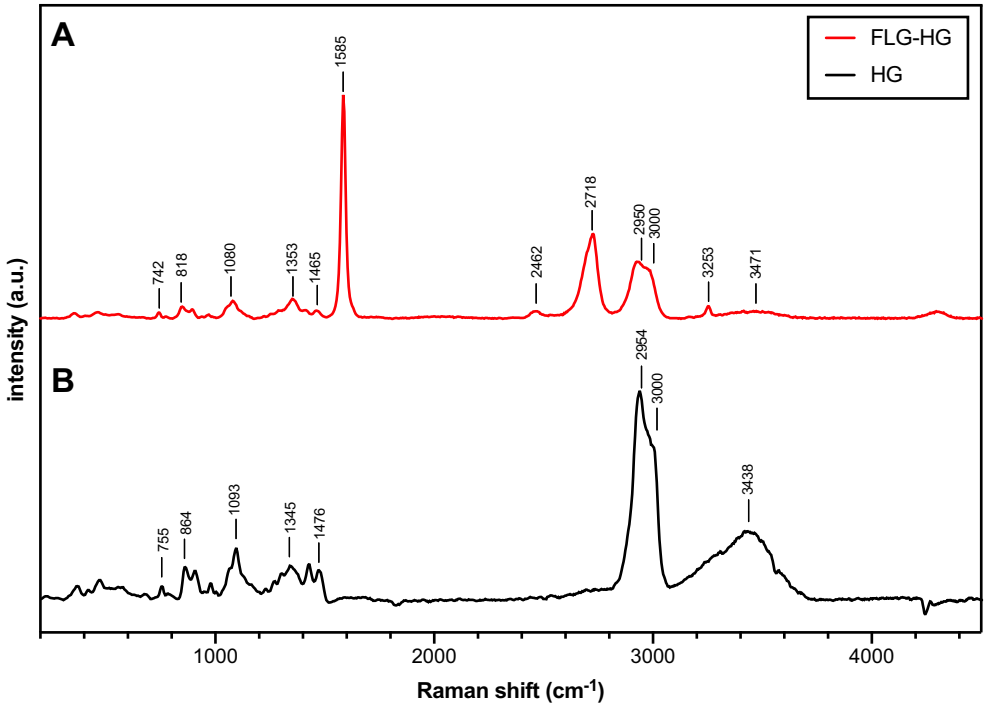

Fig. 3. Raman spectrum of FLG-laden hydrogel (A) and of neat polymeric matrix (B).

reinforcement in the mechanical properties or modulating the deformation of polymer chains due to the nanoplatelet physical hindrance. Fig. 6A shows the recorded data for HG and FLG-HG. All samples presented a storage modulus G′ approximately one order of magnitude higher than the corresponding loss modulus G″, indicating that the hydrogels are elastic rather than viscous materials, with an essentially frequency-independent behavior. Moreover, the physisorption of FLG modulates the G′ and G″ values at all investigated temperatures. At 25 °C, FLG led to an increase in the storage modulus compared to the HG reference: FLG-HG exhibited G′ = 1800 Pa, whereas HG was characterized by a value of G′ = 1200 Pa; this result could be attributed to the formed physical cross-linking points between graphene and the polymeric chains which may strengthen the gel network [53] and enhance its mechanical properties. Indeed, after FLG incorporation during the microwave-assisted synthesis, the π-lattice is responsible for the physical complexation of graphene with polymer carboxyl and hydroxyl groups, mainly through electron-based interactions and hydrogen bonds [39], limiting the movement of polymeric chains. Regarding G″, the viscous component was not significantly influenced by FLG.

On the other hand, at 37 °C and 44 °C, the graphene-laden hydrogels were characterized by lower G′ and G″ than the corresponding HG samples, showing an opposite trend compared to 25 °C. The decrease could be related to the rise of molecular mobility [54]: temperature increase promotes polymer chains elongation and the weak physical bonds (Van der Waals and hydrogen linkage) formed with FLG are minimized due to the enhanced thermal vibration mode of the π system and the consequent phonon dissipation that reduces the cross-linking feasibility in the hydrogel matrix [55]. For these reasons, FLG-HG at 37 °C and 44 °C showed comparable viscoelastic trend (G′ varies in the range 400–340 Pa and 456–377 Pa, respectively), with a slightly higher deformability at 37 °C. The latter could be explained considering the agarose and polyacrylic acid thermal response: by increasing the temperature, the polymer chains become more elongated and in particular

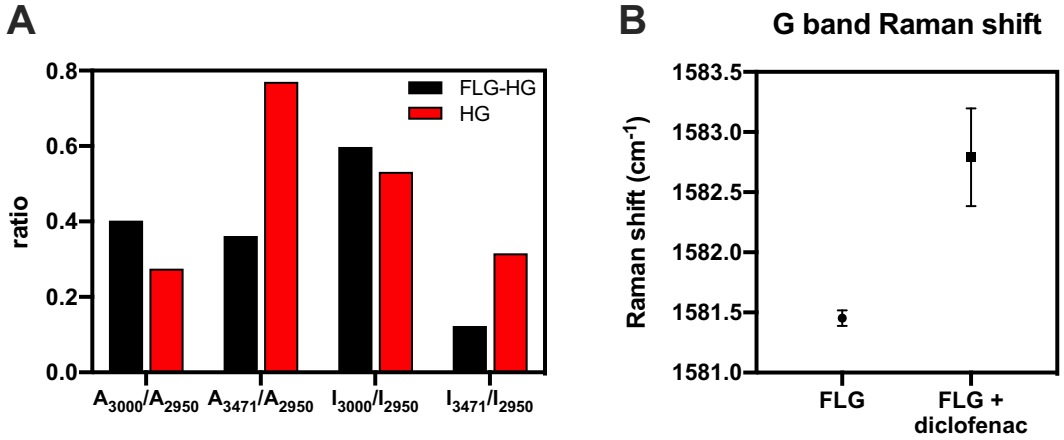

Fig. 4. A) Raman signal intensity and peak area of C—H stretching and O—H stretching due to the intramolecular interaction between FLG and polymer matrix in FLG-HG (FLG-HG, black column) compared to neat hydrogel (HG, red column). B) Raman shift values of G-band in FLG and FLG-diclofenac system. (For interpretation of the references to color in this figure legend, the reader is referred to the web version of this article.)

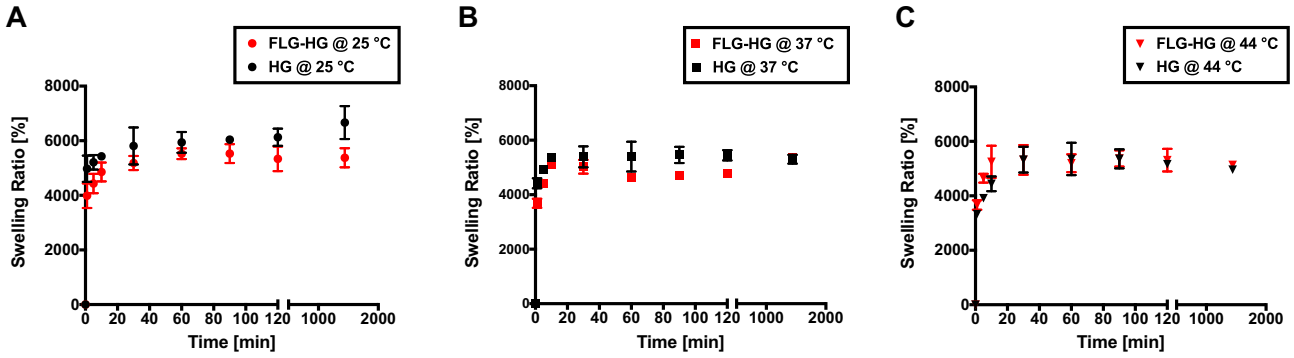

Fig. 5. Swelling behavior of FLG-HG (red) and HG (black) hydrogel at different temperatures: A) 25 °C; B) 37 °C; C) 44 °C. (For interpretation of the references to color in this figure legend, the reader is referred to the web version of this article.)

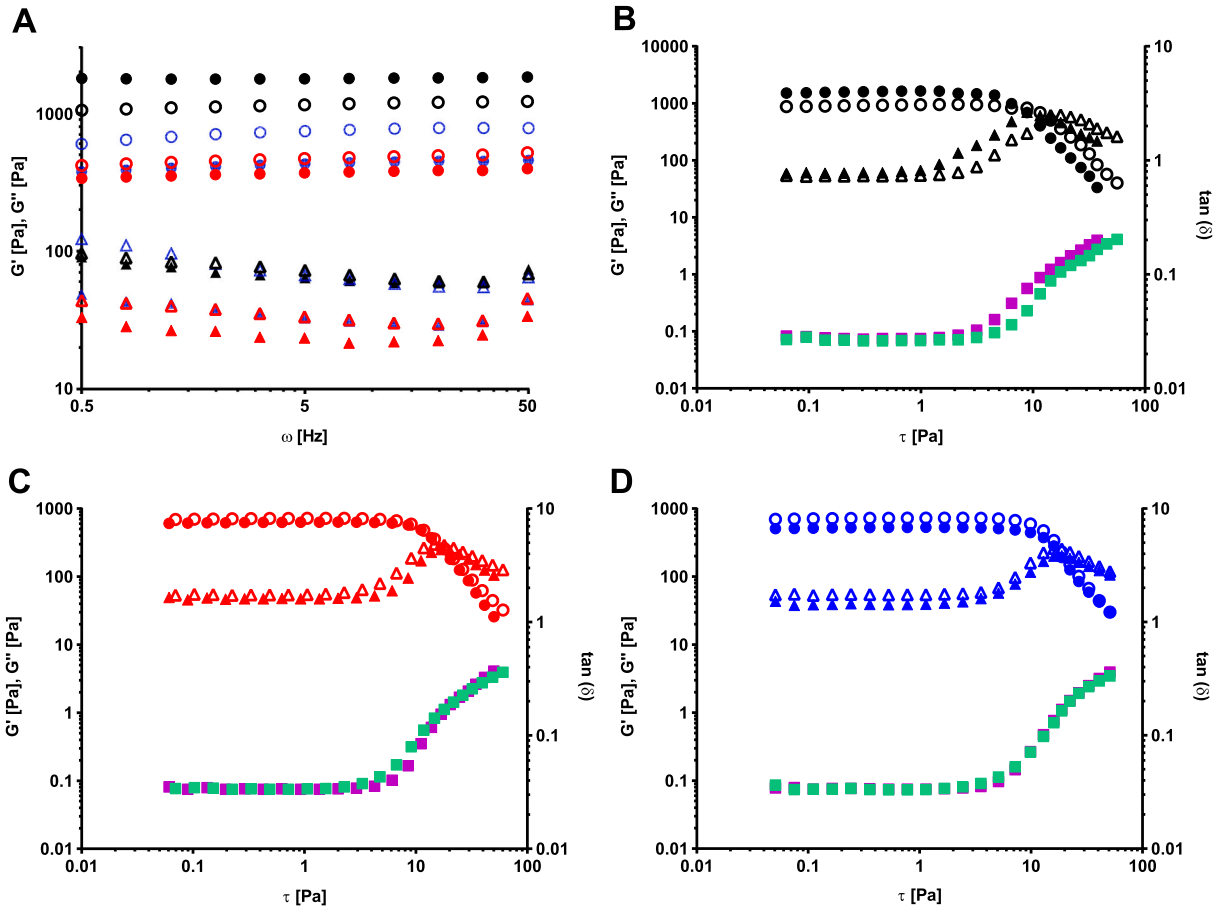

Fig. 6. Rheological behavior of graphene-laden hydrogels at 25 °C (G′ ● black, G″ ▲ black, tan(δ) ■ violet), at 37 °C (G′ ● red, G″ ▲ red, tan(δ) ■ violet) and at 44 °C (G′ ● blue, G″ ▲ blue, tan(δ) ■ violet) and hydrogels without graphene at 25 °C (G′ ○ black, G″ △ black, tan(δ) ■ green), at 37 °C (G′ ○ red, G″ △ red, tan(δ) ■ green) and at 44 °C (G′ ○ blue, G″ △ blue, tan(δ) ■ green). A) G′ and G″ trends in frequency range 0.5–50 Hz; B) crossover point at 25 °C; C) crossover point at 37 °C; D) crossover point at 44 °C. (For interpretation of the references to color in this figure legend, the reader is referred to the web version of this article.)

agarose, due to its helix conformation, tends to be entangled giving rise to micro-concentrated junctions area, assisted by formation of intramolecular hydrogen bonds [56,57]. This behavior is also oriented by the presence of chemical cross-linking points (ester bonds) between the constituents of the hydrogel matrix [58], suppressing the stress concentration during the tensile measurement [59]. As a result, the sample carried out a higher value of viscous component at 44 °C. Moreover, FLG effectively restricts the flexibility of polymer chains due to its rigid hindrance that limits the mean free path. Similar trends can be observed in HG rheology, with higher value of G″ at 37 °C and 44 °C than HG-FLG, justified by the absence of graphene constraints.

The rheology sweep test (Fig. 6B, C and D) evaluates also the flow stress value, at which the contribution of G″ is equal to G′ (crossover point) and determines the value of the material damping tan(δ), representative of the internal friction between the hydrogel meshes in that condition. At low strain, G′ and G″ of FLG-HG and HG indicate a network of packed polymeric chains and the correlation with tan(δ) confirmed for both hydrogels a solid-like response rather than a liquid-like behavior. Moreover, the intersection of storage and loss moduli occurs at similar values in both samples at 37 °C (Fig. 6C, at shear stress $\tau = 16.8$ Pa in FLG-HG and $\tau = 14.8$ Pa in HG) and 44 °C (Fig. 6D, at shear stress $\tau = 16$ Pa and $\tau = 18.8$ Pa), whereas at 25 °C the crossover

is slower in graphene-laden samples (at shear stress τ = 8.8 Pa) compared to standard hydrogel (at shear stress τ = 14.4 Pa) indicating higher stiffness in the chemical network containing FLG.

3.4. Drug release

Prior to the determination of drug release profile, the potential release of FLG from the hydrogel was ruled out (Supplementary material). Diclofenac is a nonsteroidal anti-inflammatory drug, derived from the phenylacetic acid class, with known analgesic and antipyretic properties, and commonly used in the treatments of a wide range of acute or chronic pain conditions [60,61]. Its chemical structure involves a phenylacetic acid group and a phenyl ring containing two chlorine atoms and the resulting configuration ensures the maximal twisting of the phenyl ring and provides π-π binding with other molecules or substrates. The addition of diclofenac to the FLG aqueous suspension gave rise to strong medium-range interactions among π-orbitals of the aromatic substituents and resulted in physical adsorption of single drug molecules on FLG lattice. Moreover, the inner nature of pristine graphene with defects or vacancies [62] could promote hydrogen bonds, Van der Waals and hydrophobic interactions based on the bond interaction energy and polarizability, as widely discussed in the literature [63–65]. Exploiting the magnitude of π-π interactions, we investigated the potential effect of temperature in modulating drug release profile. Fig. 7 shows the release profiles of diclofenac from FLG-HG and HG samples, at 25 °C, 37 °C and 44 °C.

The cumulative drug release from HG samples was approximately the same at each condition, defining a temperature-independent release kinetic. After 6 h, almost the entire drug payload was released from the polymer meshes. This evaluation is in accordance with the increased molecular mobility and polymer elongation, which occur at temperature exceeding RT and promote the drug escape as driven by diffusion and concentration gradient [66]. Otherwise, the presence of FLG affected the amount of released drug over time: at 25 °C a plateau at 52% was reached, whereas at 37 °C and 44 °C complete release was achieved after 6 h. This means that FLG in the hydrogel, preserving its peculiar structural features, is able to establish physical interactions with diclofenac, tuning its release in a temperature-dependent fashion: at RT, the π orbitals of FLG and diclofenac are strongly connected, probably due to the reciprocal delocalization of π electrons, and in aqueous environment they are quite stable to limit the amount of released active principle. Increasing the temperature, a distortion of this physical setup occurs, due to the increased molecular energy that overcomes the adsorption energies and enhances the dissipative forces [65]. This results in a drug desorption caused by the reduced stability of the π-π interactions. In addition, the drug release profiles within the first hours follow different trends (Fig. 8): we observed that the higher is the temperature, the higher the percentage of released diclofenac. Thus, it is possible to modulate the drug release from FLG-HG *via* temperature variation, and therefore this material represents a promising tool for therapeutic thermally-triggered approaches. A simple expression of these behaviors can be heuristically written as the sum of the diffusion-controlled and relaxation-controlled drug delivery, referring to the well-known Peppas equation [67,68] (Eq. 2):

$$\frac{M_t}{M_\infty} = kt^n \tag{2}$$

where M_t represents the cumulative amounts of drug released at time t, and M_∞ is the total amount of drug in the system (release at infinite time), k is the constant of apparent release and n the diffusion exponent. This power law is extensively used to describe the trend of the release curves [45,69,70]. The fitting of the FLG-HG experimental data shows significant differences trends in k and n values, confirming the thermal trigger effect of FLG.

In detail, the constant k shows significantly different values when comparing the experiments at 25 °C to those performed at 37 °C and 44 °C (in both cases, $p < 0.0001$), and a significant difference is also visible between 37 °C and 44 °C ($p < 0.05$). Furthermore, the diffusion exponent n shows significantly different values between RT and higher temperatures ($p < 0.05$ for 25 °C vs. 37 °C; $p < 0.01$ for 25 °C vs. 44 °C), confirming the thermal π-π effect FLG-drug in the diffusion regime. The presence of FLG affects the drug release diffusion regime naturally occurring in neat hydrogels, at all the investigated temperatures, tuning the amount of released diclofenac according to temperature increase, which led to overcome the binding energy of the attractive, noncovalent interactions between the aromatic rings. These differences in drug release profiles are not observable in HG specimens, where the trends are extremely similar at all temperatures; the influence of the graphene nanofiller is clearly detectable at 25 °C, while differences at 37 °C and 44 °C appear less marked. Overall, these data demonstrate that it is possible to perform a thermally triggered drug release without functionalization of graphene or its orthogonal grafting to specific chemical groups.

3.5. Cytotoxicity

The potential toxicity of synthetized HG and FLG-HG was assayed on hydrogel extracts in cell culture medium. Results in Fig. 9 confirm the good biocompatibility for both formulations, with an overall cell viability above 90% for extract initial concentration, that further rises to over 98% at 1:10 dilution.

3.6. Diclofenac: the effect on COX inhibition

The potential application of the proposed graphene-laden hydrogels could not be addressed without assessing the preservation of drug activity following its release. In particular, we studied its COX inhibition

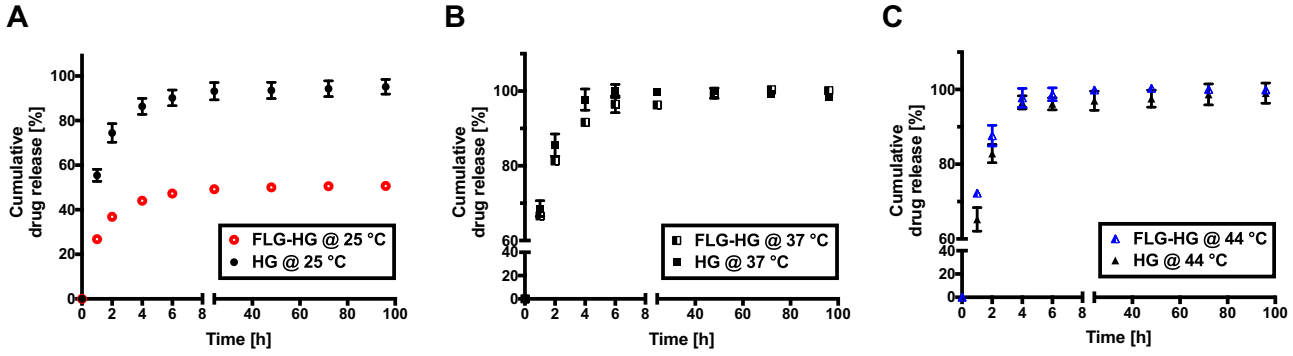

Fig. 7. A) Diclofenac release profiles in FLG-HG (○, red) and HG samples (●, black) at 25 °C; B) Diclofenac release profiles in FLG-HG (◧, black) and HG samples (■, black) at 37 °C; C) Diclofenac release profiles in FLG-HG (▲, blue), and HG samples (▲, black) at 44 °C. (For interpretation of the references to color in this figure legend, the reader is referred to the web version of this article.)

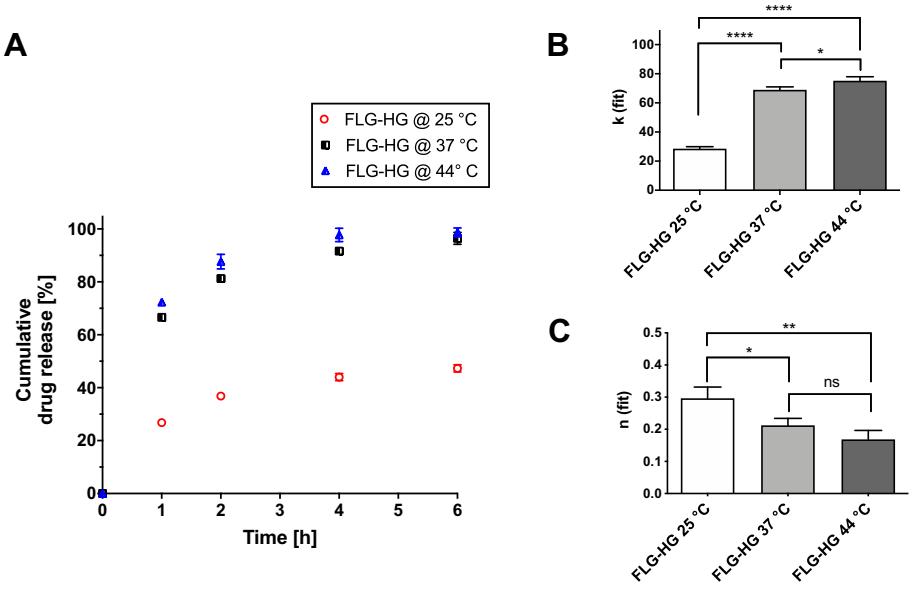

Fig. 8. A) Focus on drug release profiles in FLG-HG samples within the first 6 h: 25 °C (○, red), 37 °C (◧, black) and 44 °C (▲, blue). B, C) Evaluation of fitting parameters *k* and *n*: statistical analysis *via* one-way ANOVA. (For interpretation of the references to color in this figure legend, the reader is referred to the web version of this article.)

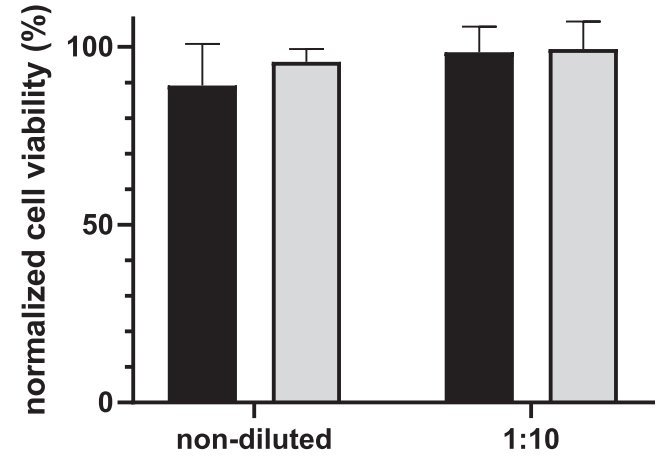

Fig. 9. Results of MTT assay performed on BALB/3T3 cells supplemented with biomaterial extracts at different titers (FLG-HG in black, HG in grey). Cell viability was normalized to that of non-treated control cells.

activity. COX is an enzyme responsible for the synthesis of prostanoids from arachidonic acid and expressing peroxidase activity. In details, COX-1 is normally involved in cellular homeostasis and it is constitutive of different cell types, whereas COX-2 is expressed under acute inflammatory conditions [71,72]. We compared the COX inhibition effect of the drug released by FLG-HG specimens after 24 h to the activity of the same amount of neat diclofenac directly administered as aqueous solution (0.25 mg/mL), using a fluorometric COX inhibition assay. The results are reported in Fig. 10.

The measurements of COX activity in the absence (hereinafter CTRL) and in the presence of the drug are plotted as RFU over time (Fig. 10A) and the fitting of the recorded data shows a significant variation ($p < 0.05$) in the slope of the regression line of CTRL compared to all other samples treated with diclofenac, but no significant differences in terms of COX inhibition have been recorded comparing pure diclofenac solution to the drug released by FLG-HG at the different temperatures (Fig. 10B). This means that the interactions between the drug and FLG did not affect the therapeutic properties of diclofenac and graphene could be considered as a useful filler to perform a thermally triggered drug release.

4. Conclusions

In this work, we propose the formulation of graphene-laden hydrogels for thermally triggered drug release. In particular, graphene was used in its pristine form, without the need of oxidation/reduction processes to reach a homogeneous distribution within the hydrogel. The resulting material meets the criteria of biocompatibility for applications in the biomedical field and its drug release profile shows an amenable dependence on the temperature in a physiologically relevant range. Furthermore, the possibility of modulating the drug delivery up to 44 °C defines these composite hydrogels as a promising tool for thermally triggered drug release in several healthcare scenarios. In light of their gelation mechanism and rheological behavior, the hydrogels may also be suitable for an application as injectable media, overcoming the main constraints related to the use of solid-like devices.

CRediT authorship contribution statement

Emanuele Mauri: Conceptualization, Methodology, Validation, Data curation, Writing - original draft, Writing - review & editing. **Aurora Salvati:** Validation, Investigation, Data curation. **Antonino Cataldo:** Conceptualization, Methodology, Validation, Investigation, Writing - original draft, Writing - review & editing. **Pamela Mozetic:** Methodology, Validation, Investigation, Visualization. **Francesco Basoli:** Methodology, Investigation, Visualization. **Franca Abbruzzese:** Validation, Investigation. **Marcella Trombetta:** Visualization, Supervision. **Stefano Bellucci:** Conceptualization, Resources, Writing - original draft, Supervision, Project administration. **Alberto Rainer:** Conceptualization, Formal analysis, Resources, Writing - original draft, Writing - review & editing, Supervision, Project administration.

Declaration of competing interest

The authors declare that they have no known competing financial interests or personal relationships that could have appeared to influence the work reported in this paper.

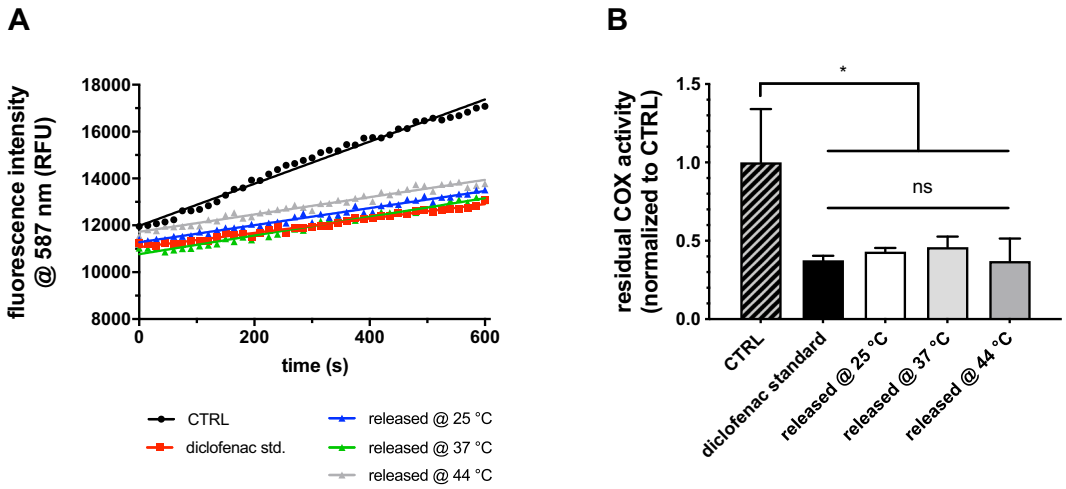

Fig. 10. A) COX activity trends in lysate samples without inhibitor (CTRL, ● black) and with the addition of: diclofenac standard (■ red), diclofenac released by FLG-HG at 25 °C (▲ blue), diclofenac released by FLG-HG at 37 °C (▲ green) and diclofenac released by FLG-HG at 44 °C (▲ grey). B) Residual COX activity (normalized to no-inhibitor CTRL) following drug administration (direct or FLG-HG-mediated administration): statistical analysis *via* one-way ANOVA. (For interpretation of the references to color in this figure legend, the reader is referred to the web version of this article.)

Acknowledgments

P.M. and A.R. are grateful to "Tecnopolo per la medicina di precisione" (TecnoMed Puglia) - Regione Puglia: DGR n.2117 dated 21/11/2018, CUP: B84I18000540002 and "Tecnopolo di Nanotecnologia e Fotonica per la Medicina di Precisione" (TECNOMED) - FISR/MIUR-CNR: delibera CIPE n.3449 dated 07/08/2017, CUP: B83B17000010001.

Appendix A. Supplementary data

Supplementary data to this article can be found online at https://doi.org/10.1016/j.msec.2020.111353.

References

[1] T.R. Hoare, D.S. Kohane, Polymer 49 (2008) 1993–2007.
[2] J.Q. Liu, L. Cui, D. Losic, Acta Biomater. 9 (2013) 9243–9257.
[3] S. Javanbakht, H. Namazi, Mater. Sci. Eng. C 87 (2018) 50–59.
[4] S. Syama, P.V. Mohanan, Nano-Micro Lett. 11 (2019) 6.
[5] M.R. Rezapour, C.W. Myung, J. Yun, A. Ghassami, N. Li, S.U. Yu, A. Hajibabaei, Y. Park, K.S. Kim, ACS Appl. Mater. Interfaces 9 (2017) 24393–24406.
[6] M. Kakran, L. Li, Key Eng. Mater. 508 (2012) 76–80.
[7] L. Nilewski, W. Sikkema, E. Samuel, A. Jalilov, K. Mendoza, R. Zhang, R. Huq, C. Beeton, M. Sharpe, D. Baskin, T. Kent, J. Tour, Abstr. Pap. Am. Chem. Soc. 253 (2017).
[8] L.Z. Feng, Z.A. Liu, Nanomedicine-UK 6 (2011) 317–324.
[9] B.M. Zhang, Y. Wang, G.X. Zhai, Mater. Sci. Eng. C 61 (2016) 953–964.
[10] F. Zheng, R. Li, Q. He, K. Koral, J. Tao, L. Fan, R. Xiang, J. Ma, N. Wang, Y. Yin, Z. Huang, P. Xu, H. Xu, Mater. Sci. Eng. C. 109 (2020) 110560.
[11] A.A. Ghawanmeh, G.A.M. Ali, H. Algarni, S.M. Sarkar, K.F. Chong, Nano Res. 12 (2019) 973–990.
[12] B. Liu, C.X. Li, Z.Y. Cheng, Z.Y. Hou, S.S. Huang, J. Lin, Biomater. Sci.-UK 4 (2016) 890–909.
[13] M. Nurunnabi, K. Parvez, M. Nafiujjaman, V. Revuri, H.A. Khan, X. Feng, Y.-k. Lee, RSC Adv. 5 (2015) 42141–42161.
[14] S.J. Cheng, H.Y. Chiu, P.V. Kumar, K.Y. Hsieh, J.W. Yang, Y.R. Lin, Y.C. Shen, G.Y. Chen, Biomater. Sci.-UK 6 (2018) 813–819.
[15] U. Dembereldorj, M. Kim, S. Kim, E.-O. Ganbold, S.Y. Lee, S.-W. Joo, J. Mater. Chem. 22 (2012) 23845–23851.
[16] C. Wang, X. Wang, T. Lu, F. Liu, B. Guo, N. Wen, Y. Du, H. Lin, J. Tang, L. Zhang, RSC Adv. 6 (2016) 22461–22468.
[17] Z. Cheng, B. Landish, Z. Chi, C. Nannan, D. Jingyu, L. Sen, L. Xiangjin, Mater. Sci. Eng. C 82 (2018) 244–252.
[18] J.M. González-Domínguez, C. Martín, Ó.J. Durá, S. Merino, E. Vázquez, ACS Appl. Mater. Interfaces 10 (2018) 1987–1995.
[19] I. Mellal, A. Oukaira, E. Kengne, A. Lakhssassi, Thermal Therapy Modalities for Cancer Treatment: A Review and Future Perspectives, (2017).
[20] S. Jha, P.K. Sharma, R. Malviya, Achiev. Life Sci. 10 (2016) 161–167.
[21] J.M.C. Bull, Int. J. Hyperth. 34 (2018) 840–852.
[22] A.L. Bredlau, M.A. McCrackin, A. Motamarry, K. Helke, C. Chen, A.-M. Broome, D. Haemmerich, Crit. Rev. Biomed. Eng. 44 (2016) 443–457.
[23] O. Ashraf, N.V. Patel, S. Hanft, S.F. Danish, World Neurosurg. 112 (2018) 166–177.
[24] E. Larrañeta, M. Henry, N.J. Irwin, J. Trotter, A.A. Perminova, R.F. Donnelly, Carbohydr. Polym. 181 (2018) 1194–1205.
[25] E. Mauri, D. Naso, A. Rossetti, E. Borghi, E. Ottaviano, G. Griffini, M. Masi, A. Sacchetti, F. Rossi, Mater. Sci. Eng. C 103 (2019) 109791.
[26] J.P. Cook, G.W. Goodall, O.V. Khutoryanskaya, V.V. Khutoryanskiy, Macromol. Rapid Commun. 33 (2012) 332–336.
[27] G. Pathak, D. Das, L. Rokhum, RSC Adv. 6 (2016) 93729–93740.
[28] R. Eyjolfsson, Drug Dev. Ind. Pharm. 26 (2000) 451–453.
[29] F. Giordano, A. Rossi, I. Pasquali, R. Bettini, E. Frigo, A. Gazzaniga, M.E. Sangalli, V. Mileo, S. Catinella, J. Therm. Anal. Calorim. 73 (2003) 509–518.
[30] A.A. Balandin, S. Ghosh, W.Z. Bao, I. Calizo, D. Teweldebrhan, F. Miao, C.N. Lau, Nano Lett. 8 (2008) 902–907.
[31] U.N. Temel, K. Somek, M. Parlak, K. Yapici, J. Therm. Anal. Calorim. 133 (2018) 907–918.
[32] A. Dabrowska, S. Bellucci, A. Cataldo, F. Micciulla, A. Huczko, Phys. Status Solidi B 251 (2014) 2599–2602.
[33] A. Maffucci, F. Micciulla, A. Cataldo, G. Miano, S. Bellucci, Nanotechnology 27 (2016).
[34] L. Pierantoni, D. Mencarelli, M. Bozzi, R. Moro, S. Moscato, L. Perregrini, F. Micciulla, A. Cataldo, S. Bellucci, IEEE Trans. Microw Theory 63 (2015) 2491–2497.
[35] D. Iannazzo, A. Pistone, C. Celesti, C. Triolo, S. Patane, S.V. Giofre, R. Romeo, I. Ziccarelli, R. Mancuso, B. Gabriele, G. Visalli, A. Facciola, A. Di Pietro, Nanomaterials-Basel 9 (2019).
[36] A. Chutia, F. Cimpoesu, H. Tsuboi, A. Miyamoto, Chem. Phys. Lett. 503 (2011) 91–96.
[37] M. Potenza, A. Cataldo, G. Bovesecchi, S. Corasaniti, P. Coppa, S. Bellucci, AIP Adv 7 (2017).
[38] N.A. Nebogatikova, I.V. Antonova, V.A. Volodin, V.Y. Prinz, Phys. E. 52 (2013) 106–111.
[39] L. Rodriguez-Perez, M.A. Herranz, N. Martin, Chem. Commun. 49 (2013) 3721–3735.
[40] L. Ferrigno, A. Cataldo, S. Sibilia, A. Maffucci, S. Bellucci, Nanotechnology 31 (2019) 075701.
[41] A.V. Kukhta, A.G. Paddubskaya, P.P. Kuzhir, S.A. Maksimenko, S.A. Vorobyova, S. Bistarelli, A. Cataldo, S. Bellucci, Synth. Met. 222 (2016) 192–197.
[42] A. Sacchetti, E. Mauri, M. Sani, M. Masi, F. Rossi, Tetrahedron Lett. 55 (2014) 6817–6820.
[43] C. Tang, L. Yin, J. Yu, C. Yin, Y. Pei, J. Appl. Polym. Sci. 104 (2007) 2785–2791.
[44] G. Calixto, A.C. Yoshii, H. Rocha e Silva, B. Stringhetti Ferreira Cury, M. Chorilli, Pharm. Dev. Technol. 20 (2015) 490–496.
[45] G. Perale, F. Rossi, E. Sundstrom, S. Bacchiega, M. Masi, G. Forloni, P. Veglianese, ACS Chem. Neurosci. 2 (2011) 336–345.
[46] P. Zarrintaj, S. Manouchehri, Z. Ahmadi, M.R. Saeb, A.M. Urbanska, D.L. Kaplan, M. Mozafari, Carbohydr. Polym. 187 (2018) 66–84.
[47] V. Georgakilas, M. Otyepka, A.B. Bourlinos, V. Chandra, N. Kim, K.C. Kemp, P. Hobza, R. Zboril, K.S. Kim, Chem. Rev. 112 (2012) 6156–6214.
[48] L.A. Belyaeva, P.M.G. van Deursen, K.I. Barbetsea, G.F. Schneider, Adv. Mater. 30 (2018) 1703274.
[49] C. Mart-N, S. Merino, J.M. Gonzalez-Dominguez, R. Rauti, L. Ballerini, M. Prato, E. Vazquez, Sci. Rep.-UK 7 (2017).
[50] B. Bahaya, D. Johnson, C. Yavuzturk, On the Effect of Graphene Nanoplatelets on Water–Graphene Nanofluid Thermal Conductivity, Viscosity, and Heat Transfer Under Laminar External Flow Conditions, (2017).

[51] Q. Chai, Y. Jiao, X. Yu, Gels 3 (2017) 6.
[52] M.C. Catoira, L. Fusaro, D. Di Francesco, M. Ramella, F. Boccafoschi, J. Mater. Sci. Mater. Med. 30 (2019) 115.
[53] S. Ganguly, D. Ray, P. Das, P.P. Maity, S. Mondal, V.K. Aswal, S. Dhara, N.C. Das, Ultrason. Sonochem. 42 (2018) 212–227.
[54] M. Bastiurea, M.S. Rodeanu, D. Dima, M. Muraresccu, G. Andrei, Dig. J. Nanomater. Bios. 10 (2015) 521–533.
[55] A.A. Balandin, Nat. Mater. 10 (2011) 569.
[56] E. Fernández, D. López, C. Mijangos, M. Duskova-Smrckova, M. Ilavsky, K. Dusek, J. Polym. Sci. Pol. Phys. 46 (2008) 322–328.
[57] B. Mao, T. Divoux, P. Snabre, J. Rheol. 60 (2016) 473–489.
[58] F. Rossi, G. Perale, G. Storti, M. Masi, J. Appl. Polym. Sci. 123 (2012) 2211–2221.
[59] J. Shen, B. Yan, T. Li, Y. Long, N. Li, M. Ye, Soft Matter 8 (2012) 1831–1836.
[60] R. Altman, B. Bosch, K. Brune, P. Patrignani, C. Young, Drugs 75 (2015) 859–877.
[61] J. Kołodziejska, M. Kołodziejczyk, Reumatologia 56 (2018) 174–183.
[62] L. Liu, M. Qing, Y. Wang, S. Chen, J. Mater. Sci. Technol. 31 (2015) 599–606.
[63] H. Tang, Y. Zhao, S. Shan, X. Yang, D. Liu, F. Cui, B. Xing, Environ. Sci. Nano 5 (2018) 2357–2367.
[64] A. Rochefort, J.D. Wuest, Langmuir 25 (2009) 210–215.
[65] S.M. Kozlov, F. Viñes, A. Görling, Carbon 50 (2012) 2482–2492.
[66] Y. Fu, W.J. Kao, Expert Opin. Drug Deliv. 7 (2010) 429–444.
[67] C. Mircioiu, V. Voicu, V. Anuta, A. Tudose, C. Celia, D. Paolino, M. Fresta, R. Sandulovici, I. Mircioiu, Pharmaceutics 11 (2019).
[68] N.A. Peppas, Pharm. Acta Helv. 60 (1985) 110–111.
[69] M.V. Ghica, M. Hirjau, D. Lupuleasa, C.E. Dinu-Pirvu, Molecules 21 (2016).
[70] C. Ferrero, A. Munoz-Ruiz, M.R. Jimenez-Castellanos, Int. J. Pharm. 202 (2000) 21–28.
[71] W.L. Xie, J.G. Chipman, D.L. Robertson, R.L. Erikson, D.L. Simmons, Prot. Natl. Acad. Sci. USA 88 (1991) 2692–2696.
[72] I. Morita, Prostag. Oth. Lipid M 68-9 (2002) 165–175.